Information Technologies on High-Energy Astrophysics:

Cosmic Ray Anisotropy using HAWC Observatory

Eduardo de la Fuente[1,3,*], *Juan Carlos* Díaz–Vélez[2,**], *Paolo* Desiati[2,***], *Jose Luis* García–Luna[3,****], *Janet* Torrealba[4,†], and *Ricardo* Gúzman–Alcála[3,‡]

[1]Information Technologies Ph.D. Program, Centro Universitario de Ciencias Económico Administrativas (CUCEA), Universidad de Guadalajara, Periferico Norte 799, Módulo L305, Los Belenes, 45100, Zapopan, Jalisco, México

[2]WIPAC & Department of Physics, University of Wisconsin–Madison, Madison, WI 53706, USA

[3]Departamento. de Física, Centro Universitario de Ciencias Exactas e Ingenierías (CUCEI), Universidad de Guadalajara, Blvd. Marcelino García Barragán 1421, esq Calzada Olímpica, 44430, Guadalajara, Jalisco, México

[4]Departamento de Ciencias Naturales y Exactas, Centro Universitario de los Valles (CUValles), Universidad de Guadalajara, Carretera Guadalajara–Ameca Km. 45.5, C.P. 46600. Ameca, Jalisco, México

Abstract. The detection of astroparticles, specially at high energies (>100 GeV), requires special techniques and instruments (telescopes or observatories), for example, those that use the Water Cherenkov radiation technique. In this paper we show an example of how Information Technologies can be used to perform maps and produce high impact results. The latter case is illustrated in the summary of the generation of a high statistics map of cosmic rays at 10 TeV in the northern sky with data collected by the High Altitude Water Cherenkov (HAWC) observatory.

1 Introduction

The field of high energy physics covers three main topics: 1.- Accelerator Physics, 2.- Astroparticles, and 3.- Nuclear Physics. Astroparticles consist of cosmic rays, gamma rays (i. e. high energy photons), and neutrinos. Multi–messenger astronomy, observationally speaking, began in 2017 [1] with the detection of recently discovered gravitational waves [2] in coincidence with electromagnetic radiation across the energy spectrum, from radio and infrared to X-rays and gamma-rays, the latter providing the link between astroparticles and multi–wavelength astronomy. An important difference between accelerator physics and astroparticle physics lies in the energy range covered by each. While artificial accelerators such as the Large Hadron Collider (LHC) are limited to energies of several TeVs, nature can reach energies up to hundreds of EeVs through astrophysical mechanisms. At energies above $\sim$ 300 GeV, direct observations of gamma rays and cosmic rays by satellite observatories are difficult due to their comparatively small effective area. However, it is possible to detect extensive air showers (EAS) composed of secondary particles produced by the interaction of gamma rays and cosmic rays in the upper atmosphere. In this sense, Earth's atmosphere acts as part of the detector and ground based detectors such as Water Cherenkov Detectors (WCD) like HAWC, Imaging Air Cherenkov Telescope (IACT) such as MAGIC and H.E.S.S., and plastic scintillator arrays, such as Grapes–3 and TA experiments, can detect the EAS particles. Detection of high-energy EAS require detectors with very large effective areas (> thousands of m^2).

Indirect observation techniques that rely on the detection of secondary particles, require the use of Information Technologies (IT), like computer modeling and Monte Carlo simulations, in order to understand the development of EAS and the detector response to such showers, for reconstructing the energy and arrival direction, and for analyzing and interpreting the observed data. In Section 2, we present a short overview of how ITs are used in high energy astrophysics studies and provide an example of how a cosmic-ray anisotropy sky map of the cosmic-ray sky was obtained combining the data of HAWC (Section 3) in the Northern hemisphere and the IceCube Neutrino Observatory in the Southern hemisphere. An actual overview of HAWC, including its upgrade and recent results, is presented by Leon–Vargas et al. [3] (these proceedings).

2 Information Technologies on High Energy Astrophysics

With simulation, we are trying to separate big and complex problems into smaller and simpler subproblems but interdependent, that is to say, the fact of performing in a computer what nature shows us, everything through a numerical convolution of many parts. If all subprocesses are known in detail, simulation produces a correct result, as

*e-mail: edfuente@gmail.com
**e-mail: juan.diazvelez@alumnos.udg.mx
***e-mail: paolo.desiati@icecube.wisc.edu
****e-mail: jlgalu2013@gmail.com
†e-mail: cjanet.torrealba@gmail.com
‡e-mail: chesirepoincar@gmail.com

in reality this situation can not occur, we must have models of reality, that is to say, simplifications, suppositions, and approximations because we are not able to have the simulation with complete parameters.

The development and detection of EAS involves several interdependent processes that despite being known (to some extent) in an individual manner, it is difficult to fully model, above all because there can be correlations between observables and dependencies, as well as statistical fluctuations. To solve this problem, we apply Monte Carlo methods in simulations in order to model the development of EAS, as well as the response of the detector, and the procedure of data reconstruction. These tasks are computationally expensive and require the use of ITs in the form of High Throughput Computing (HTC).

In general, computer simulations can serve two primary functions: 1.- understanding the development and structure of EAS to design reconstruction algorithms that extract information such as the energy and arrival direction of primary cosmic rays and gamma rays based on observables, and 2.- in the design and optimal tuning of instrumentation for detection of EAS.

2.1 Atmospheric shower simulations

A primary cosmic ray (usually high energy proton or iron nucleus) produces an EAS with three components: (1) The soft, or electromagnetic component, produces gamma rays through neutral pion decay, (2) the hard component (muons and hadrons), where charged and neutral kaons and pions decay into gamma rays, muons, neutrinos, antineutrinos, and nuclear fragments like protons and neutrons (e.g. [4–7]). For example, approximately 20% of 1 GeV muons produced at 10 km will reach sea level before decay, and (3) a nucleonic component, where high-energy nucleons, disintegration-product nucleons, and nuclear disintegration are present.

On the other hand, if a gamma ray primary hits a nucleus in the Earth's atmosphere, an electron-positron pair is produced by Coulomb interaction. These electrically charged particles, interact with other atmospheric nuclei producing secondary gamma rays via bremsstrahlung radiation ($e^{\pm} + N \longrightarrow e^{\pm} + N + \gamma$). The length scale for the energy loss of e^{-} and photons when they interact with matter (in gr cm^{-2}) is known as the radiation length. When the $e^{\pm}$ from the primary produce a secondary gamma via bremsstrahlung, we obtain one radiation length. When this secondary gamma pair-produce another $e^{\pm}$, and the resulting $e^{\pm}$ gives way to other secondary gamma via bremsstrahlung a second radiation length is obtained, and so on.

Atmospheric cosmic-ray and gamma-ray shower simulations are done using a software package originally developed for the Kascade EAS experiment program named `CORSIKA` (COsmic Ray SImulations for KAscade) [8]. Current simulations are based on `CORSIKA` v7.4000 which simulates extensive air showers caused by high energy cosmic ray particles, propagating the primary particles through the atmosphere to the ground [8]. Primary particles ranging from protons up to iron nuclei and photons are tracked through the atmosphere until they interact with air nuclei or decay. Three major types of interactions are treated in `CORSIKA`: hadronic interactions, particle decays and electromagnetic interactions.

2.2 Vavilov–Cherenkov radiation and detector response

When a charged particle (e^{-} or muons) from secondaries interacts with a polarized medium (e.g air or water), it can produce "Vavilov–Cherenkov" radiation as a result of the particle travelling faster than light in the medium ([9–12]). The HAWC instrument is modeled using a combination of community-standard simulation packages and custom software. At ground level, a `GEANT` 4 simulation (v4.10.00) of the shower particles is used to propagate the ground-level particles through the HAWC tanks and to track the Cherenkov photons to the faces of the PMTs [13]. The response of the PMTs and the calibration are approximated with a custom simulation that assumes that recorded light is faithfully detected with some efficiency and an uncertainty in the logarithm of the total charge recorded. Decorrelated single PE noise is added. The absolute PMT efficiency for detecting Cherenkov photons is established by scaling the simulated PMT response to vertical muons to match data. Most muons passing through HAWC are minimum ionizing with nearly constant energy loss. Vertical muons, therefore, are a nearly constant light source and convenient for establishing to total PMT efficiency. Simulated events are subsequently reconstructed by the same procedure as experimental data to study the performance of the algorithms.

3 The HAWC Detector

The High–Altitude Water Cherenkov (HAWC) Observatory is a unique water Cherenkov detector constructed on Sierra Negra, Puebla, México, at 4100 meters above sea level, to observe the universe in an energy range from 100 GeV to 100 TeV. The HAWC main detector consists of 300 water Cherenkov detectors (WCD), each made of a corrugated metallic cylindrical structure (7.3 m in diameter and 4.5 m high), bracing a bladder with 180,000 liters of ultra clean water and 4 photo-multiplier tubes (PMT) in its interior that work as sensors of the Cherenkov radiation produced by charged particles from extended air showers; in the center of the detector is a high quantum efficiency 10" Hamamatsu R7081-HQE PMT, surrounded by 3 8" Hamamatsu R5912 PMTs recovered from the Milagro observatory. Some HAWC main parameters are presented in Table 1. HAWC is an ideal survey instrument with a big synergy with other WCD observatories like AUGER[1], and IceCube[2].

HAWC began full operation at the end of March 2015, and it is expected to be ∼15 times more sensitive (crab) than its predecessor, the Milagro observatory. After the operation of the engineering prototype "The Verification

[1]https://www.auger.org/
[2]https://icecube.wisc.edu/

Table 1: HAWC Main Detector Parameters

Parameter	Value
Latitude	18°59′ N
Effective Area	22,000 m^2
Area of each WCD	42 m^2
Field of View	~ 2 str (15% of the whole sky)
Trigger rate	16 kHz
Detection method	cascades produced by CR and γ
Median primary energy	2 TeV
Approx. angular resolution	0.3° – 1.5°

And Measuring of the Observatory System (VAMOS)[14] built in 2011, 4 stages were considered during the modular construction of HAWC. In September 2012, the first 30 WCD were completed and still operated as engineering prototype. Then, the array was expanded to 77 WCD, then to 95 WCD, and in August 2013, the operation of a 111–tank array (HAWC–111) began. This array was operated until July 2014 and was about 3–5 times more sensitive than Milagro. On November 26, 2014, data taking began with 250 tanks (HAWC–250). The detector was expanded through the winter of 2014–2015 and full HAWC operations officially commenced on March 20, 2015. More details about the HAWC construction, performance and operation are presented in [15]. Data selected for the preliminary analysis presented here come from HAWC–250 (see [16] for details). An actual overview about the HAWC observatory, including results on cosmic ray astrophysics as well as its upgrade by installation of *outriggers*, are presented by Leon–Vargas and the HAWC Collaboration [3] (this proceedings).

4 Anisotropy in the Arrival Direction Distribution of TeV Cosmic Rays

A number of experiments have observed an anisotropy with an amplitude of 10^{-4} at energies of order 1 TeV including the Tibet ASγ [17], Super-Kamiokande [18], Milagro[19], EAS-TOP [20], MINOS [21], ARGO-YBJ [22] experiments in the Northern Hemisphere, and IceCube [23–25] and its surface air shower array IceTop [26] in the Southern Hemisphere.

There are two significant features in the observed anisotropy. The first is a large-scale structure with an amplitude of about 10^{-3}, and the second consists of several localized regions of cosmic-ray excesses with an amplitude of 10^{-4} with deficits of angular size 10° to 30°. The origin of this anisotropy is not yet well understood since it is expected that cosmic rays should lose any correlation with their original direction due to diffusion as they traverse through interstellar magnetic fields.

The anisotropy of cosmic rays is measured by computing the relative intensity as a function of equatorial coordinates (α, δ) in a sky grid of equal-area pixels using the `HEALPix` library. A binned data map $N(\alpha,\delta)_i$ with a resolution of 0.2° per bin is used to store the arrival directions of air showers recorded by the detector for each angular bin i. A reference map $\langle N\rangle(\alpha,\delta)_i$ that gives a description of the arrival direction distribution of an isotropic flux at Earth is produced by collecting all events recorded during

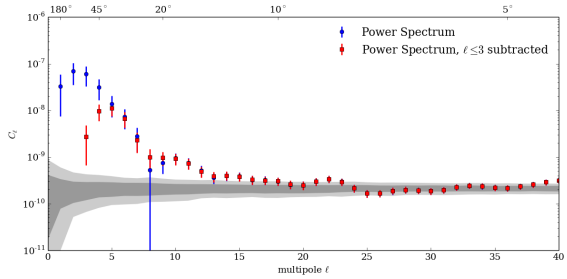

Figure 1: Angular power spectra of the unsmoothed relative intensity map before (blue) and after (red) subtracting the large–scale structure ($\ell \leq 3$). Gray errors bands show the 68% and 95% spread of the C_ℓ for isotropic data sets. Comparing the band to the data shows which *ell*-modes significantly contribute to the sky map. The error bars on the C_ℓ are the square root of the variances returned by a fit using `PolSpice`.

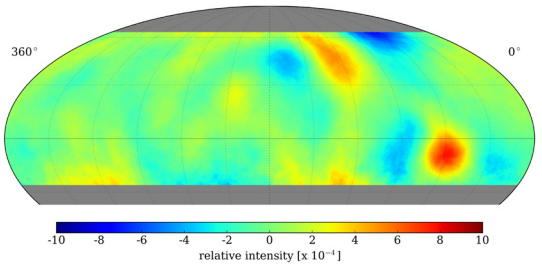

Figure 2: Relative intensity (*bottom*) of the cosmic-ray flux af-ter fit and subtraction of the dipole, quadrupole, and octupole terms from the map shown in above. The map is shown with 10° smoothing applied.

a time period Δt, and then integrating the local arrival direction distribution against the detector event rate. This is done using the direct integration technique described in [27]. This procedure effectively smooths out the true arrival direction distribution in right ascension on angular scales $\sim \Delta t \cdot 15°$ hr^{-1} and also compensates for variations in the detector rate. We calculate the deviations from isotropy using the reference by computing the relative intensity given in Eq.1

$$\delta I(\alpha,\delta)_i = \frac{\Delta N}{\langle N\rangle} = \frac{N(\alpha,\delta)_i - \langle N\rangle(\alpha,\delta)_i}{\langle N\rangle(\alpha,\delta)_i}\,, \qquad (1)$$

which gives the amplitude of deviations from the isotropic expectation in each angular bin i. The significance of the deviation can be calculated using the method of Li and Ma [28]. A choice of Δt =24 is needed to ensure a uniform angular scale as a function of declination. The analysis originally published in [29] was carried out on HAWC–111 data using Δt= 24 hr to obtain sensitivity to all angular features equally over the sky. The resulting large scale relative intensity is a combination of sidereal anisotropy and the Solar dipole effect which causes an excess of cosmic rays in the direction of the Earth's motion around the Sun. However, the two signals are difficult to disentangle unless the data cover an integer number of years of exposure such that each signal makes a complete transit in the other reference frame.

Figure 1 shows the angular power spectrum of the resulting map. The large-scale signals can be subtracted

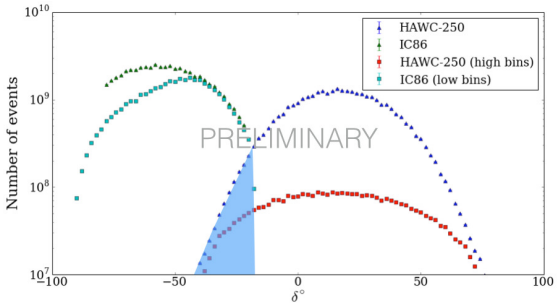

Figure 3: Distribution of events as as a function of declination for IceCube (IC) and HAWC. The shaded area corresponds to the overlapping region for both experiments [16].

from the resulting map using a multipole fit to all multipole moments $\ell \leq \ell_{max} = 3$, so we are left with the small-scale structure in the sidereal frame. The residual structure will contain power at angular scales less than $180°/\ell_{max} = 60°$.

The resulting small-scale anisotropy map is shown in Figure 2. A 10° smoothing has been applied. Three significant features remain. These excesses coincide with the $10° - 20°$ regions of cosmic-ray excess first observed by Milagro [30] (Regions A and B) as well as a third region observed only by ARGO-YBJ [31] (Region C).

Connecting the northern and southern measurements would eliminate biases from partial sky coverage. No clear connection of the small-scale anisotropy that is present in both hemispheres has been made yet. The published IceCube maps are of higher energy (20 TeV median) than HAWC and other northern measurements. Unlike it's predecessor Milagro (35.88° N latitude), HAWC has a field of view that overlaps with that of IceCube (see Figure 3). Because of this, there is ongoingwork to combine HAWC and IceCube data using cuts to bring their median energies closer to a central value [32, 33].

Acknowledgements

E. de la F. wishes to thank financial support from CUCEA–Secretaria Academica–Coordinación de Postgrados, U de G. J.C.D.V and E. de la F. also deeply thank Stefan Westerhoff (RIP) for guiding, teaching and contributions to the knowledge and rising of the Astroparticles field on Jalisco, México.

References

[1] Abbott, B. P., et al., Astrophys. J. Lett. **848**, L12–L71 (2017).
[2] Abbott, B. P., et al., Phys. Rev. Lett. **119**, 161101–161118 (2017).
[3] H. León–Vargas, The HAWC Collaboration, EPJ Web of Conf. **these proceedings** (2018)
[4] H. J. Bhabha and W. Heitler, Proceedings of the Royal Society of London A. **159**, 432–458 (1937)
[5] J. F. Carlson and]. R. Oppenheimer, Phys. Rev. **61**, 220–231 (1937)
[6] G.T. Zatsepin, Doklady Akademii Nauk SSSR **67**, 993–1001 (1949)
[7] Greisen, K. 1960, Annual Review of Nuclear and Particle Science **10**, 63–68
[8] D. Heck, et al., Kernforschungszentrum Karlsruhe KfK **5196 B**, (1993)
[9] P. A. Cerenkov, Doklady Akad. Nauk SSSR **2**, 451–455 (1934)
[10] S. I. Vavilov, Doklady Akad. Nauk SSSR **2**, 457–459 (1934)
[11] P. A. Cerenkov, Phys. Rev. **52** 378–381 (1937)
[12] Tamm, I.E., and Frank, I.M., Doklady Akad. Nauk SSSR **14**, 107–112 (1937)
[13] , Agostinelli, et al. Nucl. Inst. Meth. Phys. Res. Sec. **506**, 250 (2003)
[14] Abeysekara et al., Astroparticle Physics **62**, 125–133 (2015)
[15] A. Smith et al., Proceedings of Science **ICRC2015**, 1–8 (2015)
[16] J. Díaz-Vélez et al., Proceedings of Science **ICRC2015**, 1–8 (2015)
[17] M. Amenomori et al., Astrophys. J. Lett. **626**, L29–L32 (2005)
[18] G. Guillian et al., Phys. Rev. D **75**, 062003 (2007)
[19] A. A. Abdo et al., Phys. Rev. Lett. **101**, 221101 (2008)
[20] M. Aglietta et al., Astrophys. J. Lett. **692**, L130–L133 (2009)
[21] J. De Jong, International Cosmic Ray Conference **4**, 46 (2011)
[22] G. Di Sciascio, EPJ Web of Conf. **52**, 4004, (2013)
[23] R. Abbasi et al., Astrophys. J. Lett. **718**, L194–L198, (2010)
[24] R. Abbasi et al., Astrophys. J. **740**, 16, (2011)
[25] R. Abbasi et al., Astrophys. J. **746**, 33, (2012)
[26] M. G. Aartsen et al., Astrophys. J. **765**, 55, (2013)
[27] R. W. Atkins et al., Astrophys. J. **595**, 803–811, (2003)
[28] T.-P. Li and Y.-Q. Ma, Astrophys. J. **272**, 317–324, (1983)
[29] A. Abeysekara et al., Astrophys. J. **796**, 108, (2014)
[30] A. A. Abdo et al., Astrophys. J. **698**, 2121–2130 (2009)
[31] B. Bartoli et al., Phys.Rev. **D88**, 082001 (2013)
[32] J. C. Díaz–Vélez, Ph. D. Thesis, CUValles, Universidad de Guadalajara (2018)
[33] J. C. Díaz–Vélez et al., Astrophys. J. to be submitted (2018)